

• Original Paper •

Interannual Climate Variability Change during the Medieval Climate Anomaly and Little Ice Age in PMIP3 Last Millennium Simulations

Kaiqing YANG^{1,4} and Dabang JIANG^{*1,2,3}

¹*Institute of Atmospheric Physics, Chinese Academy of Sciences, Beijing 100029, China*

²*Joint Laboratory for Climate and Environmental Change at Chengdu University of Information Technology, Chengdu 610225, China*

³*CAS Center for Excellence in Tibetan Plateau Earth Sciences, Beijing 100101, China*

⁴*University of Chinese Academy of Sciences, Beijing 100049, China*

(Received 27 March 2016; revised 6 September 2016; accepted 24 October 2016)

ABSTRACT

In this study, we analyzed numerical experiments undertaken by 10 climate models participating in PMIP3 (Paleoclimate Modelling Intercomparison Project Phase 3) to examine the changes in interannual temperature variability and coefficient of variation (CV) of interannual precipitation in the warm period of the Medieval Climate Anomaly (MCA) and the cold period of the Little Ice Age (LIA). With respect to the past millennium period, the MCA temperature variability decreases by 2.0% on average over the globe, and most of the decreases occur in low latitudes. In the LIA, temperature variability increases by a global average of 0.6%, which occurs primarily in the high latitudes of Eurasia and the western Pacific. For the CV of interannual precipitation, regional-scale changes are more significant than changes at the global scale, with a pattern of increased (decreased) CV in the midlatitudes of Eurasia and the northwestern Pacific in the MCA (LIA). The CV change ranges from -7.0% to 4.3% (from -6.3% to 5.4%), with a global average of -0.5% (-0.07%) in the MCA (LIA). Also, the variability changes are considerably larger in December–January–February with respect to both temperature and precipitation.

Key words: interannual variability, last millennium, Medieval Climate Anomaly, Little Ice Age

Citation: Yang, K. Q., and D. B. Jiang, 2017: Interannual climate variability change during the Medieval Climate Anomaly and Little Ice Age in PMIP3 last millennium simulations. *Adv. Atmos. Sci.*, **34**(4), 497–508, doi: 10.1007/s00376-016-6075-1.

1. Introduction

The last millennium is a most recent key period in paleoclimatology. The climate, which was barely different from that of today, and the increasing anthropogenic activities in this period (Schmidt et al., 2011; Braconnot et al., 2012; IPCC, 2013), both make it a valuable reference for current climate research. Moreover, the sufficient levels of proxy data and reliable instrumental observations overlap in temporal terms, which provides opportunities for determining causes and mechanisms of climate change at various timescales. As a consequence, developing a better understanding of the climate in the last millennium has attracted much scientific interest in recent years.

Geological evidence-based reconstruction and numerical modelling are two main approaches for paleoclimate research. For the former, scientists collect information from single sites or from collections of natural archives, such as

tree rings, marine and lake sediments, corals, and annually resolved ice cores, and transform them into climate signals to reflect climate behavior. Most reconstructed time series (e.g., Jones and Mann, 2004; Juckes et al., 2007; Mann, 2007; Mann et al., 2009; Cook et al., 2013) and spatial patterns (e.g., Mann et al., 2009; Ljungqvist et al., 2012; Ahmed et al., 2013; Neukom et al., 2014) of temperature indicate a moderately warmer “Medieval Climate Anomaly” (MCA) period, followed by a generally cooler “Little Ice Age” (LIA) condition over the last millennium. And records for precipitation also similarly suggest these two typical periods, although they are mostly restricted to regional scales and contain discrepancies from site to site. For example, during the MCA, the western United States exhibits continual drought (Cook et al., 2004), and northeastern China (Ren, 1998) and the northeastern Tibetan Plateau (Yang et al., 2014) show opposite wet conditions. Whereas, in the case of the LIA, more precipitation is presented in the Qinling Mountains of central China (Tan et al., 2009) and the northeastern Tibetan Plateau (Yang et al., 2014). These reconstructions open the door for climate research on the last millennium. However, they are also ac-

* Corresponding author: Dabang JIANG
Email: jiangdb@mail.iap.ac.cn

accompanied by large uncertainty. Because all proxy data are indirect measurements of climate, their reliability varies with the choices of proxy data and algorithms. Besides, the sparse distribution of proxy sites makes it difficult to characterize climate on the global scale.

Numerical experiments performed by climate models make up for the weaknesses of proxy reconstructions. In this respect, the MCA and LIA periods have been reproduced reliably (e.g., Ammann et al., 2007; Landrum et al., 2013). By comparing paleoclimate data and model simulations, on the one hand, model/reconstruction performance has been enhanced (e.g., Bothe et al., 2013; Fernández-Donado et al., 2013; Neukom et al., 2014); on the other hand, an advance in understanding the formation of the LIA has also been made by Miller et al. (2012) that it was possibly induced by decadal-paced volcanism and sustained by subsequent sea-ice/ocean feedbacks, rather than having resulted from solar irradiance changes. Furthermore, flexibility in the complexity of models and the design of experiments enables a more in-depth examination of these two unique periods, primarily with respect to the attribution of climate changes. Specifically, it has been pointed out that both solar irradiance (e.g., Bard and Frank, 2006; Ammann et al., 2007; Swingedouw et al., 2011) and internal mechanisms (e.g., Hunt, 1998; Goosse et al., 2012; Fernández-Donado et al., 2013) were responsible for long-term climate change, whereas volcanic eruptions provided more of an influence on decadal to annual timescales (e.g., Hegerl et al., 2003; Yang and Jiang, 2015), and anthropogenic forcing became a major factor from the middle of the 20th century (e.g., Crowley, 2000; Jones and Mann, 2004; Jiang et al., 2015). Moreover, internal feedbacks have been found to make a greater contribution than external forcings on regional and local scales (e.g., Goosse et al., 2005), and impact differently between interannual and centennial–millennial scale variations (Liu et al., 2011).

The climatology of the last millennium has recently been widely documented. Little, however, is known about the interannual climate variability in this period. The intensity of the interannual climate variability is highly important, since it is closely related to the occurrence of extreme events (Katz and Brown, 1992; Fan et al., 2014), and the interannual variability change can reflect the variation in the stability of the

climate system. Thus, it is of interest to investigate interannual climate variability in the last millennium.

In the above context, the present paper presents an analysis based upon multi-model simulations to illustrate (1) the climatology of the interannual variability over the last millennium, and (2) the changes in the interannual variability in the relatively warm (MCA) and cold (LIA) climate backgrounds.

2. Data and method

2.1. Model and observational data

In this study, we examined all available simulations of the last millennium in the Paleoclimate Modelling Intercomparison Project Phase 3 (PMIP3), as performed by 11 climate models. MIROC-ESM was excluded, because it is not properly spun-up and shows long-term climate drift (Bothe et al., 2013; Gupta et al., 2013); hence, it has problems in reproducing the MCA and LIA climates. The remaining 10 models are listed in Table 1, along with their horizontal and vertical resolutions and time spans. All the models cover the analyzed millennium period of 851–1849, with the exception of FGOALS-gl, whose run is from 1000 to 1999. This is due to its different application of external forcings in volcanic aerosols and solar irradiance (Zhou et al., 2011), which are not recommended by the PMIP3 design (Schmidt et al., 2011). In addition, we considered only one (R124, with the most same boundary conditions as the other models) of the eight GISS-E2-R ensembles (R121–128) to avoid overemphasizing the influence of this model.

The 10 models show a simulated globally cooling trend in the last millennium (Fig. 1), which agrees with available reconstructions (e.g., Jones and Mann, 2004; Juckes et al., 2007; Mann et al., 2009; Ahmed et al., 2013; Neukom et al., 2014). On this basis, for convenience of further analysis, we referred to the definitions in IPCC (2013) together with the results from proxy-based reconstructions, and chose the periods 950–1250 and 1450–1849 as the MCA and LIA, respectively, although their precise timings are still controversial in the literature. Therein, the MCA is 1000–1250 for FGOALS-gl because of the different time span addressed above. Furthermore, the temperature differences

Table 1. Details of the model simulations used in this study. Model IDs with asterisks represent those with historical runs covering 1901–2000 for assessment.

Model ID	Model name	Country	Atmospheric resolution (lon × lat, vertical layers)	Time span
01*	BCC-CSM1.1 (Wu, 2012)	China	~ 2.8° × 2.8°, L26	850–2000 AD
02*	CCSM4 (Gent et al., 2011)	USA	1.25° × ~ 0.9°, L26	850–1850 AD
03	CSIRO Mk3L-1-2 (Phipps et al., 2011)	Australia	~ 5.6° × ~ 3.2°, L18	851–1850 AD
04	FGOALS-gl (Zhou et al., 2011)	China	5.0° × ~ 4.0°, L26	1000–1999 AD
05	FGOALS-s2 (Bao et al., 2010)	China	~ 2.8° × ~ 1.7°, L26	850–1850 AD
06*	GISS-E2-R (Schmidt et al., 2006)	USA	2.5° × 2.0°, L40	850–1850 AD
07*	HadCM3 (Gordon et al., 2000)	UK	3.75° × 2.5°, L19	850–1850 AD
08*	IPSL-CM5A-LR (Dufresne et al., 2012)	France	3.75° × ~ 1.9°, L39	850–1850 AD
09*	MPI-ESM-P (Giorgetta et al., 2013)	Germany	~ 1.9° × ~ 1.9°, L47	850–1849 AD
10*	MRI-CGCM3 (Yukimoto et al., 2012)	Japan	~ 1.1° × ~ 1.1°, L48	850–1850 AD

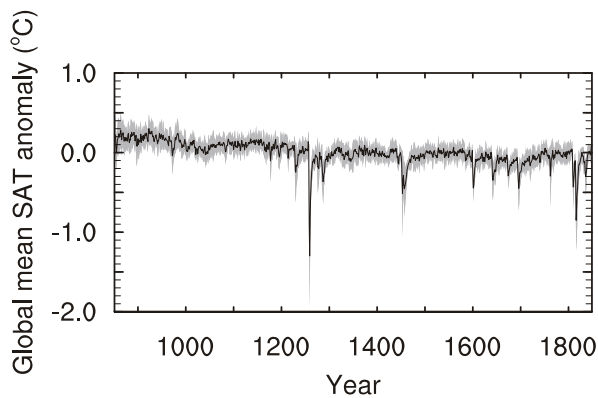


Fig. 1. Time series of the annual global mean surface air temperature anomaly (units: °C) during the period 851–1849. Black solid line and gray shading represent the ensemble mean and one standard deviation of the 10 models, respectively.

between these two periods vary from 0.3°C (FGOALS-s2) to 0.5°C (MRI-CGCM3) across the models.

The observational data used to assess the ability of the climate models in simulating global temperature and precipitation climatology were from the Climate Research Unit TS3.10 monthly datasets (Harris et al., 2014) for the period 1901–2000 (referred to simply as the observation). These datasets were calculated on high-resolution ($0.5^{\circ} \times 0.5^{\circ}$) grids, based on an archive of monthly mean data provided by more than 4000 land-based weather stations distributed around the world.

2.2. Method

Based on the range of horizontal resolutions for all the models, we first re-gridded (through bilinear interpolation for resolutions from low to high, and distance-weighted average re-mapping for the ones from high to low) the simulation and observational data to a relatively mid-range level of $2.0^{\circ} \times 2.0^{\circ}$ for further intercomparison. Then, we linearly removed the long-term trends and decadal filtered the data using an 11-yr high-pass Butterworth filter to obtain the interannual climate signals. We defined the interannual variability as the standard deviation of the obtained interannual, annual or seasonal means, and performed seasonal analysis according to the common division of December–January–February (DJF), March–April–May (MAM), June–July–August (JJA), and September–October–November (SON).

2.3. Evaluation of the climate models

To build confidence in the climate models regarding their ability to reproduce the climatology of the interannual climate variability, we calculated the spatial correlation coefficients and normalized centered rooted mean square errors (RMSEs) between each simulation and observation on land for the 1901–2000 period. The results, presented as Taylor diagrams, reveal that, for the interannual variability of annual temperature (precipitation), the spatial correlation coefficients of the models vary from 0.77 to 0.91 (0.69 to 0.78),

and the normalized centered RMSEs vary from 0.5 to 0.7 (0.6 to 0.8) (Figs. 2a and c). On the seasonal scale (Figs. 2b and d), the models show relatively large scatter and inferior skill, especially for interannual temperature variability in JJA. The spatial correlation coefficients for the interannual variability of seasonal temperature range between 0.53 and 0.92 (0.53 and 0.78 in JJA), and the normalized centered RMSEs range between 0.4 and 1.8 (0.9 and 1.8 in JJA). With respect to seasonal precipitation, the spatial correlation coefficients range from 0.61 to 0.79 and the normalized centered RMSEs from 0.6 to 1.3. Therefore, we considered that most models are able to capture the main spatial features of the interannual variability climatology reasonably well, and thus used the ensemble mean of all 10 models to represent the overall simulation in this study.

3. Results

3.1. Interannual temperature variability

3.1.1. Interannual temperature variability over the last millennium

The ensemble mean of the climatology for interannual temperature variability averages 0.4°C over the globe, with a land contribution of 0.6°C and an ocean contribution of 0.4°C . Also, the variability of the Northern Hemisphere (average of 0.5°C) is greater than that of the Southern Hemisphere (average of 0.4°C). Spatially, the distribution patterns differ little among individual models, and the region where discrepancy mainly occurs is the eastern tropical Pacific, with only two (CSIRO Mk3L-1-2 and GISS-E2-R) of the 10 models not supporting the ensemble mean feature. Figure 3a shows that the interannual variability is large at high latitudes and small at low latitudes, which is also characteristic in past millennium (e.g., Zorita et al., 2005) and pre-industrial (e.g., Jiang et al., 2016) climate simulations. The largest variabilities are located in the Greenland Sea (maximum value of 1.5°C), Barents Sea, and Bering Strait in the Northern Hemisphere, and the Amundsen Sea and Weddell Sea in the Southern Hemisphere. When averaged zonally, the curves present a maximum land–ocean contrast at midlatitudes. This is consistent with earlier simulation work, in which it was stated that the atmosphere–ocean coupling is responsible for the land–ocean variability difference at midlatitudes (Barsugli and Battisti, 1998).

On the seasonal scale (Figs. 3b–e), the interannual variabilities are relatively larger than the annual mean, with global averages of 0.8°C , 0.7°C , 0.6°C and 0.7°C in DJF, MAM, JJA and SON, respectively. Such seasonal amplification is supported by the reconstructions undertaken by Mann et al. (2000) and Luterbacher et al. (2004), in which the standard deviation of winter temperature in Europe is larger than that of summer. More specifically, the greater seasonal values come from the increased variability over both land and ocean, particularly for land in the mid and low latitudes, and especially for the DJF period. With respect to the spatial distribution in DJF, the variability is extremely large in the

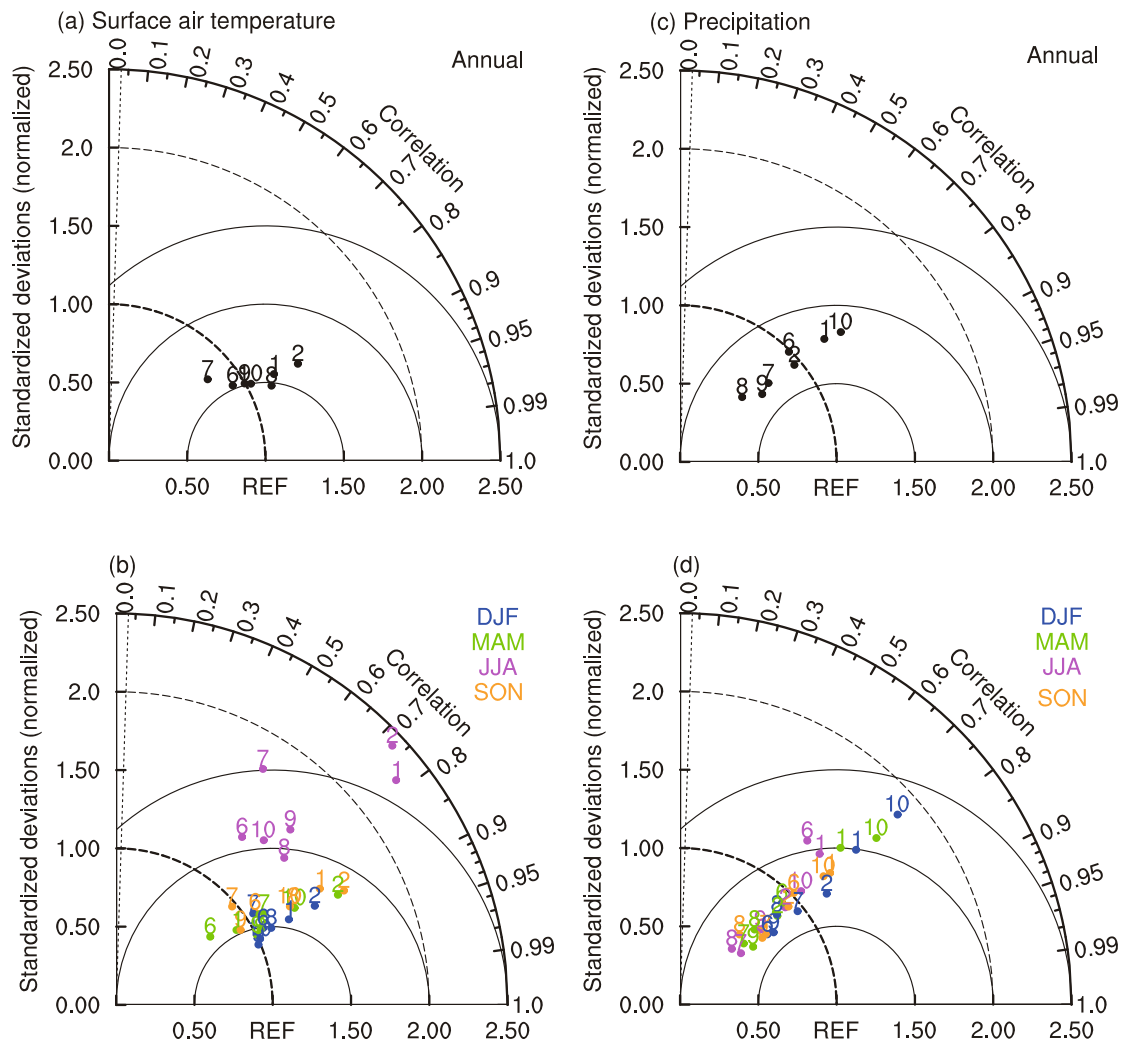


Fig. 2. Taylor diagrams (Taylor, 2001) displaying normalized pattern statistics of interannual climatological (a, c) annual and (b, d) seasonal mean (a, b) surface air temperature and (c, d) precipitation, over the global land area, between seven model simulations and observations for 1901–2000. Each number represents a model ID (see Table 1). Black, blue, green, red and orange dots show simulations of annual, DJF, MAM, JJA and SON means, respectively. The references (REF) indicate observations. The correlation coefficient between a model and the reference is given by the azimuthal position of the model, with the oblique dotted lines showing the 99% confidence level. The normalized standard deviation of a model is the radial distance from the origin, with cambered dotted lines showing the values of 1.00 and 2.00. The normalized centered root-mean-square difference between a model and the reference is their distance apart, with the cambered solid lines showing values of 0.05, 1.00 and 1.50 for all the figures. In short, the shorter the distance between a number and REF, the better the performance of the corresponding model.

northern high latitudes, and there are two large-value centers, located in northwestern Eurasia and northern North America. By JJA, the variability in the southern high latitudes becomes relatively larger, of which that over the ocean is larger than that over land. To a certain degree, this seasonal cycle reflects the role of solar radiation balance in driving interannual variability.

3.1.2. Changes in interannual temperature variability in the MCA and LIA

Since the geographical distribution of climate change is very different from the global mean change, and because it is local- rather than global-scale climate change that affects

human activities and the natural ecosystem, an indicator with local influence would be more appropriate for investigations of variability change, especially for those on precipitation addressed below. Therefore, in the following discussion, we utilize the percentage change, the ratio of variability change (difference between the MCA or LIA and the 851–1849 period) to variability climatology in the 851–1849 period, to characterize the relative change amplitude in one specific area.

With respect to the millennium background, Fig. 4a shows the ensemble mean of the interannual variability in annual temperature in the MCA to vary by -2.0% globally (ranging from -9.6% to 3.1%), due to similar decreases over

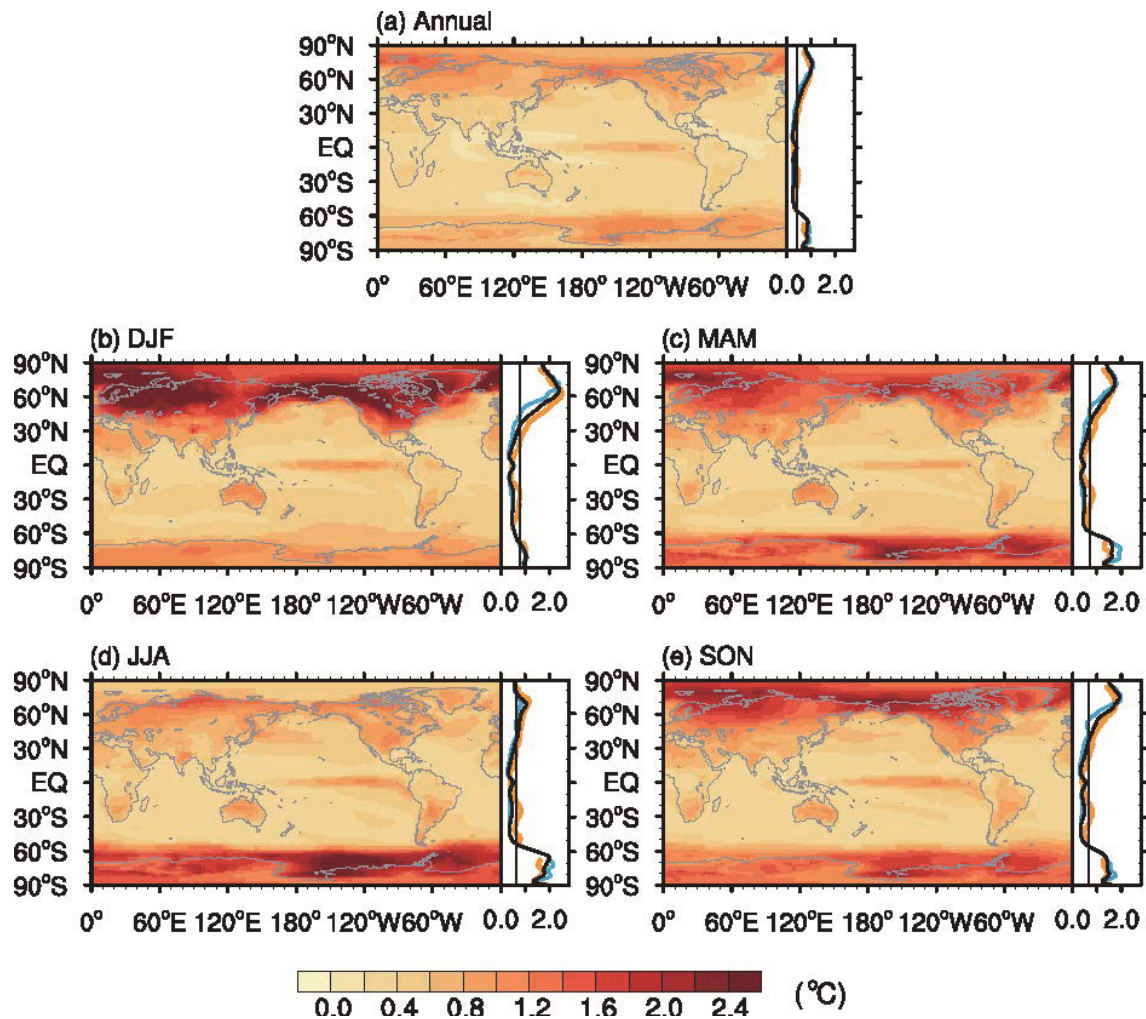


Fig. 3. Interannual surface air temperature variability (units: °C) over the period 851–1849 based on the ensemble mean of 10 models in the (a) annual, (b) DJF, (c) MAM, (d) JJA and (e) SON period, respectively. The black, blue and yellow curves in the right-hand panels are the zonal means over the global, ocean and land areas, respectively. The vertical, long solid line represents the global mean.

both ocean (–2.0%) and land (–2.1%). Geographically, for individual models, variability changes exhibit diverse distributional features, which result from the various physical and dynamic frameworks of the models and the fine differences between the chosen external forcings. In general, model consistency is better in the Northern Hemisphere than in the Southern Hemisphere, indicating a better knowledge of physical processes and interactions in the former. In terms of the ensemble mean, the variability shows an overall decrease in most of the Northern Hemisphere and low-latitude Southern Hemisphere, with the low-latitude (except for the eastern tropical Pacific) changes being most significant. Centers of decline occur in the tropical Indian Ocean, the western tropical Pacific, tropical Atlantic, and the Bering Strait. This wide-ranging decline thus leads to a zonal negative change in the tropical regions, which differs slightly between land and ocean. However, we note that this distribution contains information on both absolute variability change and background millennial variability, and when the signal of millennial variability is removed, comparable magnitude across regions is

displayed.

On the seasonal scale (Figs. 4b–e), the area and intensity of the MCA decline are both weaker than those of the annual mean, with global averages of –1.2%, –1.1%, –1.4% and –1.4% in DJF, MAM, JJA and SON, respectively. The weakening is obviously severe on land rather than over ocean, reflecting a sensitive land response. Compared to the annual mean, the decreased variability is more concentrated over the low-latitude oceans.

Although the above results seem to indicate an interannual variability decline in the MCA, whether it is statistically significant remains unclear. Thus, we applied the *F*-test to determine the significance of the variability difference between the MCA and the whole millennium period. The results (Figs. 5a–e) show the proportions of the global grids with a statistically significant increase (decrease) to be 1.5%, 1.5%, 1.4%, 2.0% and 1.7% (9.9%, 6.8%, 6.6%, 9.0% and 7.1%) in the annual, DJF, MAM, JJA and SON periods, respectively. Note that the CCSM4 simulation proportions are nearly three times greater than those of the other models.

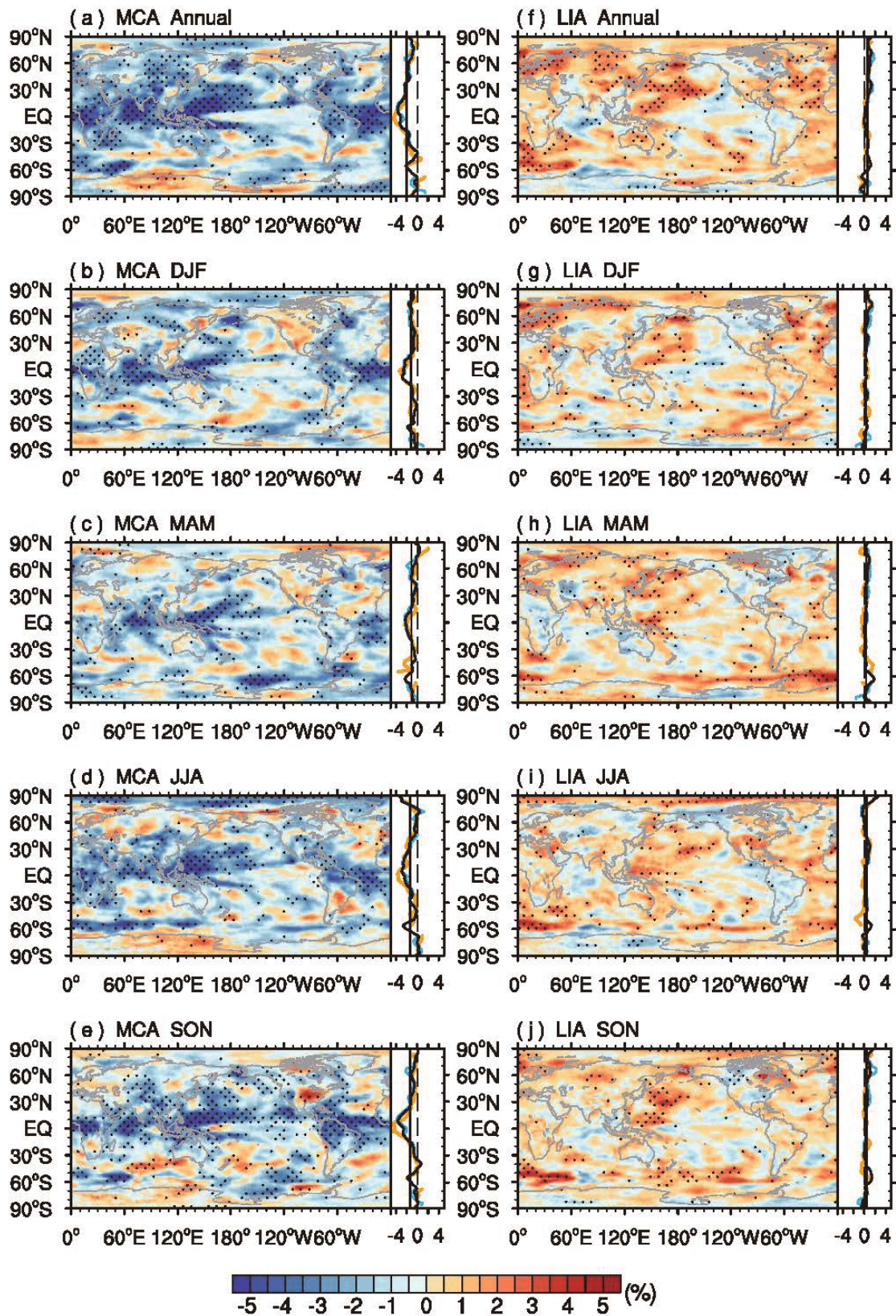


Fig. 4. Percentage change in interannual variability of surface air temperature between (a–e) the MCA or (f–j) the LIA and the period 851–1849 based on the ensemble mean of 10 models. Panels (a, f), (b, g), (c, h), (d, i) and (e, j) represent the annual, DJF, MAM, JJA and SON periods, respectively. The black, blue and yellow curves, and the vertical, long solid lines are the same as in Fig. 3. The vertical, long dashed line shows zero. The dotted areas represent regions where at least 60% of the models share the same sign of changes.

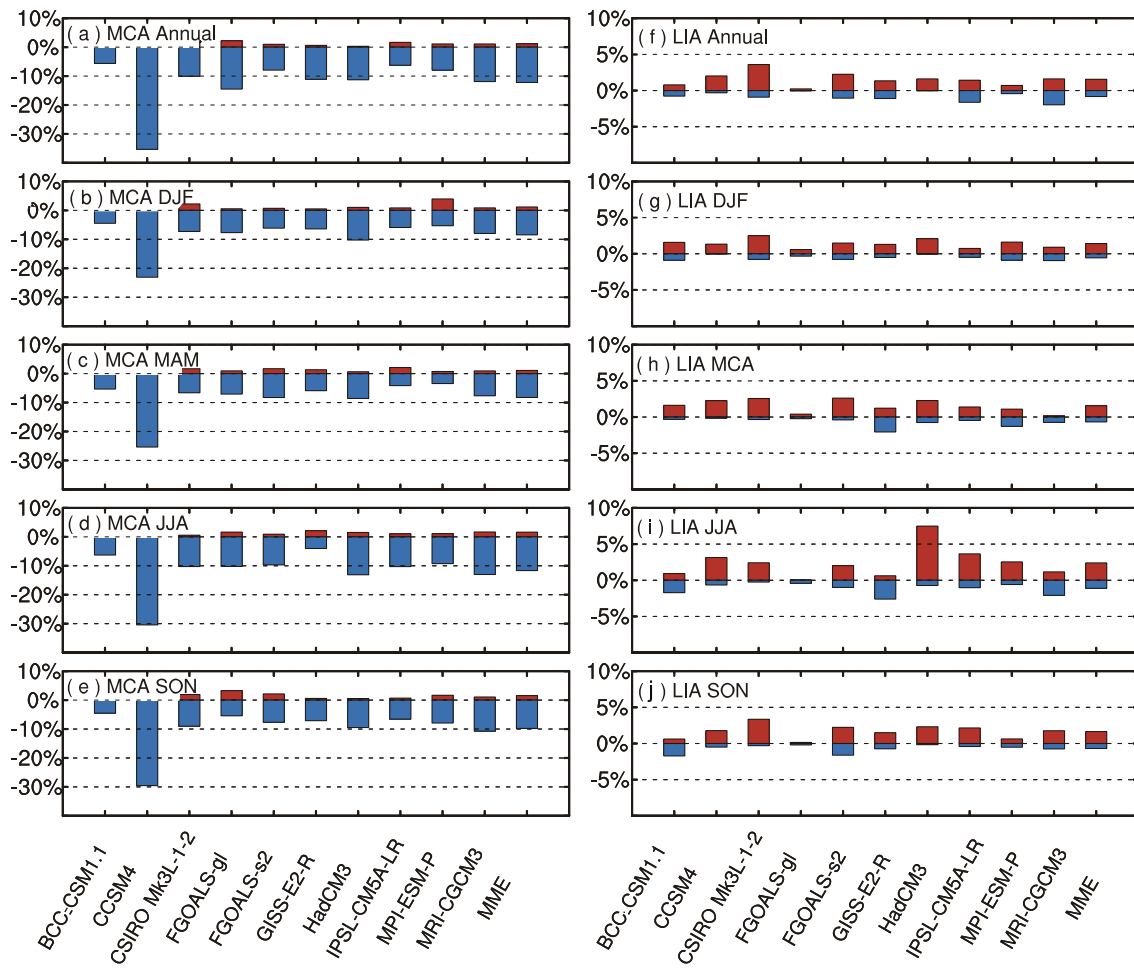


Fig. 5. Percentages of global grids that have statistically different interannual surface air temperature variability in (a–e) the MCA or in (f–j) the LIA from those over the period 851–1849, for the individual models and the ensemble mean (MME) of 10 models. Panels (a, f), (b, g), (c, h), (d, i) and (e, j) represent the annual, DJF, MAM, JJA and SON periods, respectively. The red (blue) bars indicate positive (negative) variability changes. The results are based on the *F*-test with the 90% confidence level.

Such a large response has previously been discussed by Landrum et al. (2013) and Yang and Jiang (2015), implying that this model is particularly sensitive to external forcings. Based on the above, we can conclude that the interannual temperature variability in the relatively warm MCA period decreased with respect to the entire last millennium.

As for the LIA, the interannual variability of annual temperature increases regionally (Fig. 4f) in most models. The ratios range from –3.6% to 4.8%, with a global average of only 0.6% due to the scattered distribution. Land and ocean respectively contribute 0.5% and 0.6% to this increase. Spatially, a greater increase mostly occurs in the Northern Hemisphere (specifically, in high-latitude Eurasia, the midlatitudes of the northwestern Pacific, and the North Atlantic); while for the Southern Hemisphere, the increase mainly appears in the southeastern Pacific and Atlantic–Indian Ocean to the south of South Africa. Additionally, the zonal mean curves show little difference between land and ocean at most latitudes. Disregarding the influence of the background variability over the millennium, the absolute variability change is spatially

comparable.

Seasonally (Figs. 4g–j), the global mean increases fall to 0.4% for all four seasons. Although the increase comes from both land and ocean, the land represents the major origin. In detail, the increase primarily occurs in high-latitude Eurasia, the midlatitudes of the northern Pacific, and the northern Atlantic in DJF; the northwestern Pacific and high latitudes of the southern Atlantic in MAM; the northwestern Pacific and the Atlantic in JJA; and the northwestern Pacific and the high-latitude oceans around Antarctica in SON. Again, we applied the *F*-test to determine the statistical significance of these results in the LIA. As shown in Figs. 5f–j, only 1.5%, 1.1%, 1.2%, 1.7% and 1.4% (1.1%, 0.8%, 0.7%, 1.3% and 1.0%) of the global grids significantly increase (decrease) in the annual, DJF, MAM, JJA and SON periods, respectively. Thus, the interannual temperature variability in the relatively cold LIA period increased slightly.

Taken together, the above results indicate that the interannual temperature variability increased in the MCA and decreased in the LIA. This is generally consistent with the

assessment of CCSM4 simulations (Landrum et al., 2013). Furthermore, the preference for regional features rather than global variations in the whole millennium has also been previously reported by Ahmed et al. (2013).

3.2. Interannual precipitation variability over the last millennium

In simulations of the last millennium, the interannual precipitation variability generally enlarges with decreases in latitude. Spatially, the largest variability occurs in the tropical oceans (with the exception of the eastern Pacific between 5°S – 5°N), with a regional average exceeding 0.8 mm d^{-1} (1.6 mm d^{-1}) for the annual (seasonal) mean, followed by relatively large values in tropical Africa, tropical South America, the midlatitudes of the northern Pacific, and the midlatitudes of the Atlantic. Comparing this pattern with that of absolute precipitation, we find that overall the two patterns overlap. However, since the magnitude of precipitation has a broad location-dependent span, a same variability change in different regions would be of diverse meanings. Therefore, to better examine the precipitation variability on the global

scale, the subsequent analysis utilize the coefficient of variation (CV), defined as the ratio of the standard deviation to the mean, to characterize the precipitation variation rather than variability. By this means, the large impact of the precipitation distribution is reduced, and the change in the CV of interannual precipitation can measure the interannual precipitation variability change with less regional effect. Also, the change in the CV of interannual precipitation is the percentage change addressed above.

3.2.1. CV of interannual precipitation over the last millennium

With respect to the annual mean precipitation, the CV over the millennium period varies from 0.08 to 1.60 and averages at 0.22 globally, and the regional average over land (ocean) is 0.25 (0.21). Individual models simulate similar spatial patterns, with only IPSL-CM5A-LR not supporting the ensemble mean feature in the eastern tropical Pacific. This implies agreement among the models in reproducing the climatology of precipitation variability. The distribution of the annual CV (Fig. 6a) is opposite to that for the precipita-

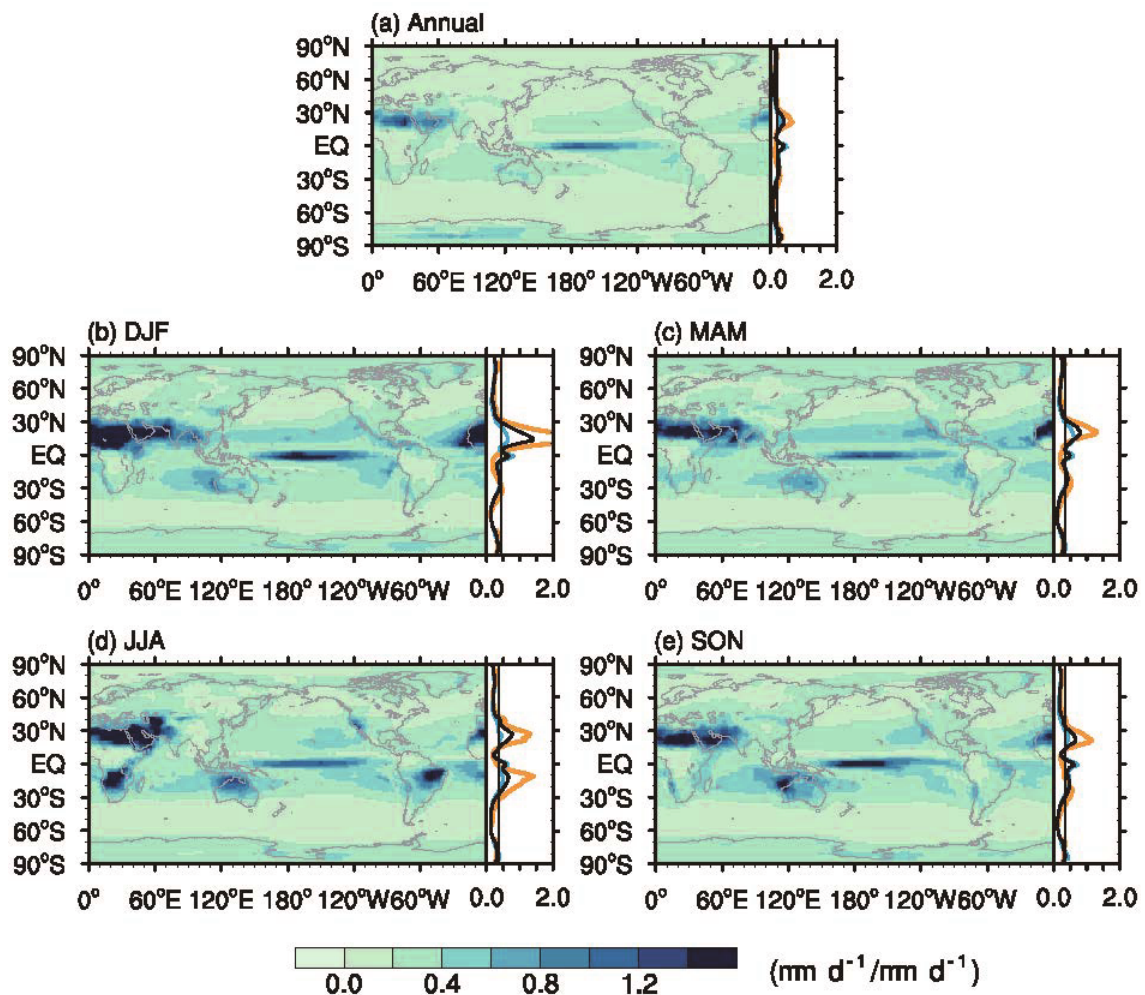


Fig. 6. Coefficient of variation of interannual precipitation over the period 851–1849 based on the ensemble mean of 10 models in the (a) annual, (b) DJF, (c) MAM, (d) JJA and (e) SON periods, respectively. The black, blue and yellow curves, and vertical, long solid lines are the same as in Fig. 3.

tion field, where large CVs generally correspond to small precipitation values. The largest CVs occur in the Sahara Desert, Iran Plateau, and central tropical Pacific—roughly the driest areas worldwide; the larger CVs are located in the low-latitude oceans, together with Australia, Greenland, and the Rose and Weddell seas; the smallest CVs occur in most of the monsoon regions and high latitudes. Zonally, the CV is large at low latitudes and small at high latitudes, and the land–ocean contrast mostly originates from areas with extreme CVs.

The seasonal CV is larger overall than the annual mean (Figs. 6b–e), and this comes considerably from more the land rather than the ocean contribution in low latitudes, especially in DJF. The global averages are 0.42, 0.34, 0.37 and 0.34 (with ranges of 0.09–8.77, 0.09–2.96, 0.09–4.47 and 0.09–2.74) in DJF, MAM, JJA and SON, respectively. For DJF, large CVs centering on dry regions in the Northern Hemisphere (the Sahara and Iran Plateau) reach their peaks, and as JJA arrives, these extremes decrease and those in the Southern Hemisphere increase, specifically in South Africa, northern Australia, and eastern South America.

3.2.2. Changes in the CV of interannual precipitation in the MCA and LIA

As reported in a precipitation reconstruction (Yang et al., 2014) and an up-to-date reanalysis dataset investigation (Fan et al., 2014), the change in the interannual variability of precipitation is due to local processes rather than continent-scale dynamics. In this study, the results obtained from multi-model simulations consistently present an uneven distribution of interannual CV change worldwide (Fig. 7). However, though individual models show diverse distributions of CV change, the inter-model agreement is better in midlatitude Eurasia, along the southeastern edge of the Sahara and in the northeastern Pacific.

With reference to the millennium period, the MCA (LIA) change in the interannual CV for the annual mean precipitation (Figs. 7a and f) ranges from -7.0% to 4.3% (-6.3% to 5.4%). Due to the nearly half-and-half percentage of positive and negative values, the global average varies only by -0.5% (-0.07%), and the land and ocean averages are -0.4% and -0.5% (-0.1% and -0.5%), respectively. Zonal curves fluctuate with latitude, with little difference between land and ocean. Spatially, the CV displays overall opposite signs over Eurasia between the MCA and LIA.

Seasonally (Figs. 7b–e and 7g–j), the ranges of the CV change are wider. In DJF, MAM, JJA and SON in the MCA, they vary from -25.4% to 16.9% , from -11.8% to 11.7% , from -13.7% to 10.4% , and from -13.6% to 10.4% , respectively; and in the LIA, they are from -23.4% to 14.6% , from -10.9% to 9.5% , from -15.4% to 13.3% , and from -9.1% to 7.9% , respectively—all with close to zero global averages. In DJF, most model simulations show decreased CVs in eastern China and the northwestern Pacific and increased CVs in western Eurasia in the MCA, and the opposite generally holds for the LIA. For the other three seasons, the changes are also contradictory in the above areas, with overall CV

increases (decreases) in the MCA (LIA). Furthermore, disagreement is evident in both polar regions, where zonal mean values are negative for the annual mean, but positive in the seasonal results. This non-synchronicity phenomenon has been confirmed in a cooling trend simulation of CCSM4 from the MCA to the LIA (Landrum et al., 2013), and, to a certain degree, might result from polar amplification (Masson-Delmotte et al., 2006) in some of the polar areas. Altogether, the CV change in interannual precipitation is mainly regionally and seasonally distributed, and tends to increase (decrease) in the MCA (LIA) over Eurasia and the northwestern Pacific.

4. Conclusion and discussion

In this study, the simulations of 10 climate models archived in PMIP3 were applied to examine firstly the climatology of interannual temperature variability and the CV of interannual precipitation during the last millennium, and secondly, their changes in the relatively warm period of the MCA and the cold period of the LIA. The primary findings were as follows:

(1) The interannual temperature variability increases with increasing latitude and is large in the Northern Hemisphere, and the CV of interannual precipitation increases with decreasing latitude and shows extreme large values in dry areas. Regarding annual means averaged over the globe, the interannual temperature variability is 0.4°C and the CV of interannual precipitation is 0.22. Both levels are smaller than the seasonal values, and the largest-value season in both cases is DJF.

(2) With respect to the millennium period, the interannual temperature variability decreases (increases) in most of the low latitudes (high-latitude Eurasia and the western Pacific) in the MCA (LIA), with a global mean average of -2.0% (0.6%). Both the intensity and area of the changes decrease on the seasonal scale, which are due primarily to the reduced land variability, especially in DJF.

(3) Compared to the millennium period, the change in CV of interannual precipitation is highly region- and season-dependent. The CV changes vary from -7.0% to 4.3% and from -6.3% to 5.4% (global averages of -0.5% and -0.07%) in the MCA and LIA, respectively. It tends to increase (decrease) in midlatitude Eurasia and the northwestern Pacific in the MCA (LIA).

Note that climate variation involves both internal feedback and external forcing. Previous work (Yang and Jiang, 2015) indicated that the zonal mean interannual temperature (precipitation) variability has a latitude-based (little) response to volcanic forcing. This is consistent with the conclusion in the present study that, overall, the temperature variability of the MCA (LIA), with less (more) volcanic eruptions, decreased (increased). Meanwhile, as shown in Fig. 7, the variability in precipitation also supports more regional changes than global-scale variations; thus, the leading regional signals probably contributed the weak volcanic re-

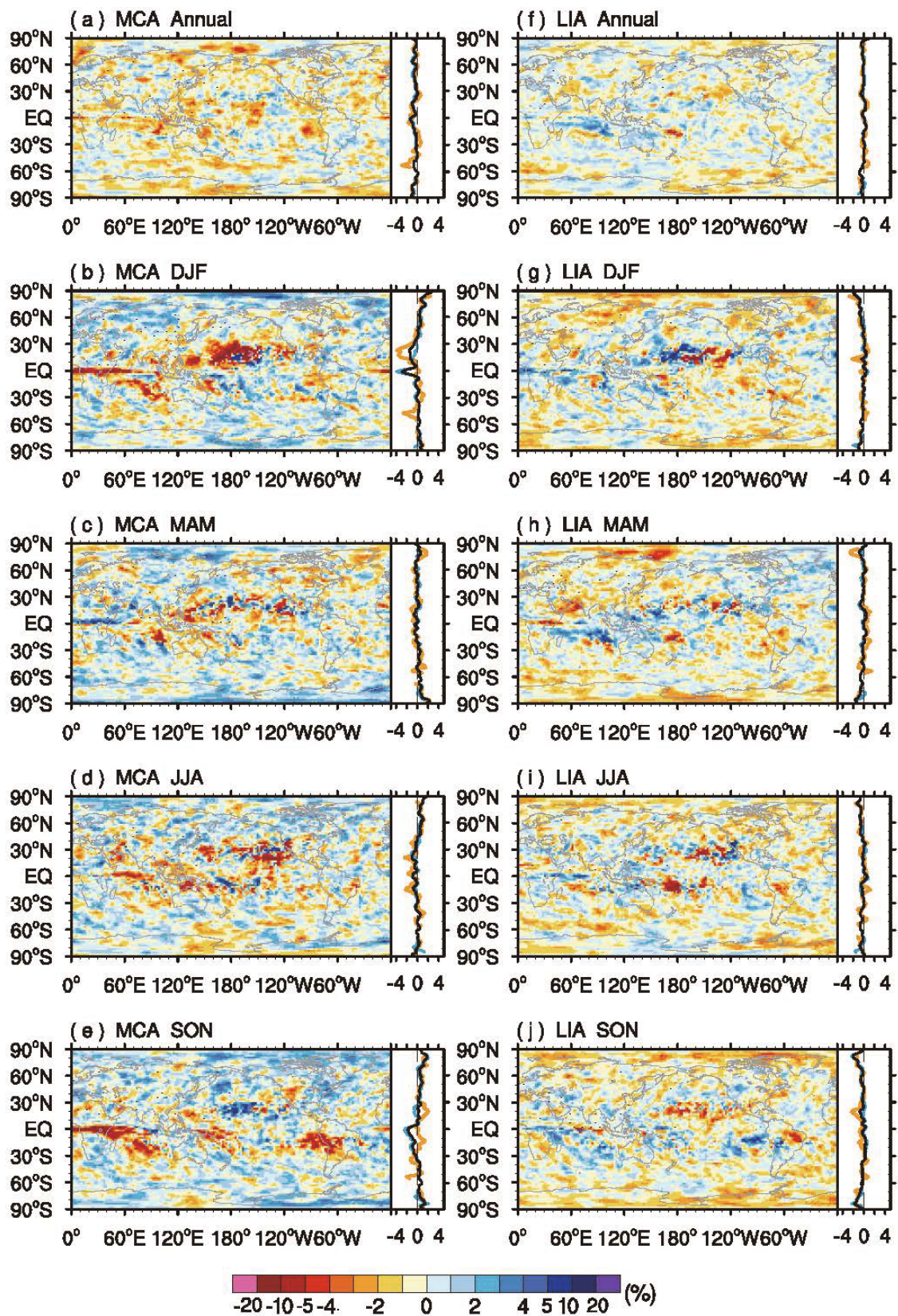


Fig. 7. Percentage change in the coefficient of variation of interannual precipitation between (a–e) the MCA or (f–j) the LIA and the period 851–1849 based on the ensemble mean of 10 models. Panels (a, f), (b, g), (c, h), (d, i) and (e, j) represent the annual, DJF, MAM, JJA and SON periods, respectively. The black, blue and yellow curves are the same as in Fig. 3. The vertical, long dashed line shows zero. The dotted areas represent regions where at least 60% of the models share the same sign of changes.

sponse in the zonal and global mean states. Explosive volcanism affects the climate system chiefly by changing the radiation balance. Recent studies have suggested that volcanic eruptions can strongly influence the surface temperature gradient, which led to the Sahelian drought (Haywood et al., 2013), as well as modulate the circulation rather than moisture content, consequently leading to precipitation change (Liu et al., 2016). Moreover, it has been found that the intensity and location of an eruption can influence the volcanic impacts. Volcanic aerosols from a highly active event can be injected directly into the stratosphere and transport poleward in both hemispheres, thus covering the entire globe eventually (e.g., Schneider et al., 2009). Volcanoes in tropical regions are known to have greater influences than those in extratropical regions (e.g., Schneider et al., 2009), and those in one hemisphere can barely affect the monsoonal precipitation in the other hemisphere (Liu et al., 2016). The present study provides support for a volcanic impact on climate variability on the interannual time scale for two periods of a few centuries, and motivates further analysis on understanding volcano-induced climate change. Finally, recent studies have reported that the skill of climate models in simulating variability is inferior to that for simulating climatology (Braconnot et al., 2012; IPCC, 2013), and the different MCA time spans of FGOALS-g1 with the other models both may imply uncertainty in our results.

Acknowledgements. We acknowledge the climate modeling groups (listed in Table 1) for producing and sharing their model outputs. This research was supported by the National Natural Science Foundation of China (Grant No. 41421004) and the National Key Research and Development Program of China (Grant No. 2016YFA0600704).

REFERENCES

- Ahmed, M., and Coauthors, 2013: Continental-scale temperature variability during the past two millennia. *Nature Geo.*, **6**, 339–346.
- Ammann, C. M., F. Joos, D. S. Schimel, B. L. Otto-Bliesner, and R. A. Tomas, 2007: Solar influence on climate during the past millennium: Results from transient simulations with the NCAR climate system model. *Proceedings of the National Academy of Sciences of the United States of America*, **104**(10), 3713–3718.
- Bao, Q., G. X. Wu, Y. M. Liu, J. Yang, Z. Z. Wang, and T. J. Zhou, 2010: An introduction to the coupled model FGOALS1.1-s and its performance in East Asia. *Adv. Atmos. Sci.*, **27**(5), 1131–1142, doi: 10.1007/s00376-010-9177-1.
- Bard, E., and M. Frank, 2006: Climate change and solar variability: What's new under the sun? *Earth and Planetary Science Letters*, **248**(1–2), 1–14.
- Barsugli, J. J., and D. S. Battisti, 1998: The basic effects of atmosphere–ocean thermal coupling on midlatitude variability. *J. Atmos. Sci.*, **55**(4), 477–493.
- Bothe, O., J. H. Jungclaus, and D. Zanchettin, 2013: Consistency of the multi-model CMIP5/PMIP3-past1000 ensemble. *Climate of the Past*, **9**(6), 2471–2487.
- Braconnot, P., and Coauthors, 2012: Evaluation of climate models using palaeoclimatic data. *Nature Climate Change*, **2**(6), 417–424.
- Cook, E. R., C. A. Woodhouse, C. M. Eakin, D. M. Meko, and D. W. Stahle, 2004: Long-term aridity changes in the western United States. *Science*, **306**(5698), 1015–1018.
- Cook, E. R., P. J. Krusic, K. J. Anchukaitis, B. M. Buckley, T. Nakatsuka, and M. Sano, 2013: Tree-ring reconstructed summer temperature anomalies for temperate East Asia since 800 C.E. *Climate Dyn.*, **41**(11–12), 2957–2972.
- Crowley, T. J., 2000: Causes of climate change over the past 1000 years. *Science*, **289**(5477), 270–277.
- Dufresne, J. -L., and Coauthors, 2012: Climate change projections using the IPSL-CM5 Earth System Model: From CMIP3 to CMIP5. *Climate Dyn.*, **40**(9–10), 2123–2165.
- Fan, K., Z. Q. Xu, and B. Q. Tian, 2014: Has the intensity of the interannual variability in summer rainfall over South China remarkably increased? *Meteor. Atmos. Phys.*, **124**(1–2), 23–32.
- Fernández-Donado, L., and Coauthors, 2013: Large-scale temperature response to external forcing in simulations and reconstructions of the last millennium. *Climate of the Past*, **9**(1), 393–421.
- Gent, P. R., and Coauthors, 2011: The Community Climate System Model Version 4. *J. Climate*, **24**(19), 4973–4991.
- Giorgetta, M. A., and Coauthors, 2013: Climate and carbon cycle changes from 1850 to 2100 in MPI-ESM simulations for the Coupled Model Intercomparison Project phase 5. *J. Adv. Model. Earth Syst.*, **5**, 572–597.
- Goosse, H., H. Renssen, A. Timmermann, and R. S. Bradley, 2005: Internal and forced climate variability during the last millennium: A model-data comparison using ensemble simulations. *Quaternary Science Reviews*, **24**(12–13), 1345–1360.
- Goosse, H., E. Cresspin, S. Dubinkina, M. F. Loutre, M. E. Mann, H. Renssen, Y. Sallaz-Damaz, and D. Shindell, 2012: The role of forcing and internal dynamics in explaining the “Medieval Climate Anomaly”. *Climate Dyn.*, **39**(12), 2847–2866.
- Gordon, C., and Coauthors, 2000: The simulation of SST, sea ice extents and ocean heat transports in a version of the Hadley Centre coupled model without flux adjustments. *Climate Dyn.*, **16**, 147–168.
- Gupta, A. S., N. C. Jourdain, J. N. Brown, and D. Monselesan, 2013: Climate drift in the CMIP5 models. *J. Climate*, **26**(21), 8597–8615.
- Harris, I., P. D. Jones, T. J. Osborn, and D. H. Lister, 2014: Updated high-resolution grids of monthly climatic observations—the CRU TS3.10 dataset. *Int. J. Climatol.*, **34**(3), 623–642.
- Haywood, J. M., A. J. N. Bellouin, and D. Stephenson, 2013: Asymmetric forcing from stratospheric aerosols impacts Sahelian rainfall. *Nature Climate Change*, **3**, 660–665.
- Hegerl, G. C., T. J. Crowley, S. K. Baum, K.-Y. Kim, and W. T. Hyde, 2003: Detection of volcanic, solar and greenhouse gas signals in paleo-reconstructions of northern hemispheric temperature. *Geophys. Res. Lett.*, **30**(5), doi: 10.1029/2002GL016635.
- Hunt, B. G., 1998: Natural climatic variability as an explanation for historical climatic fluctuations. *Climatic Change*, **38**(2), 133–157.
- IPCC, 2013: *Climate Change 2013: The Physical Science Basis. Contribution of Working Group I to the Fifth Assessment Report of the Intergovernmental Panel on Climate Change*, T. F.

- Stocker et al., Eds., Cambridge University Press, Cambridge, United Kingdom and New York, NY, USA, 1535 pp.
- Jiang, D. B., and Coauthors, 2015: Paleoclimate modeling in China: A review. *Adv. Atmos. Sci.*, **32**(2), 250–275, doi: 10.1007/s00376-014-0002-0.
- Jiang, D. B., Y. Sui, and X. M. Lang, 2016: Timing and associated climate change of a 2°C global warming. *Int. J. Climatol.*, **36**(14), 4512–4522.
- Jones, P. D., and M. E. Mann, 2004: Climate over past millennia. *Rev. Geophys.*, **42**(2), doi: 10.1029/2003RG000143.
- Juckes, M. N., and Coauthors, 2007: Millennial temperature reconstruction intercomparison and evaluation. *Climate of the Past*, **3**(4), 591–609.
- Katz, R. W., and B. G. Brown, 1992: Extreme events in a changing climate: Variability is more important than averages. *Climatic Change*, **21**(3), 289–302.
- Landrum, L., B. L. Otto-Bliesner, E. R. Wahl, A. Conley, P. J. Lawrence, N. Rosenbloom, and H. Y. Teng, 2013: Last millennium climate and its variability in CCSM4. *J. Climate*, **26**(4), 1085–1111.
- Liu, F., J. Chai, B. Wang, J. Liu, X. Zhang, and Z. Y. Wang, 2016: Global monsoon precipitation responses to large volcanic eruptions. *Sci. Rep.*, **6**, 24331.
- Liu, J., B. Wang, H. L. Wang, X. Y. Kuang, and R. Y. Ti, 2011: Forced response of the East Asian summer rainfall over the past millennium: Results from a coupled model simulation. *Climate Dyn.*, **36**, 323–336.
- Ljungqvist, F. C., P. J. Krusic, G. Brattström, and H. S. Sundqvist, 2012: Northern Hemisphere temperature patterns in the last 12 centuries. *Climate of the Past*, **8**(1), 227–249.
- Luterbacher, J., D. Dietrich, E. Xoplaki, M. Grosjean, and H. Wanner, 2004: European seasonal and annual temperature variability, trends, and extremes since 1500. *Science*, **303**(5663), 1499–1503.
- Mann, M. E., 2007: Climate over the past two millennia. *Annual Review of Earth and Planetary Sciences*, **35**(1), 111–136.
- Mann, M. E., E. Gille, R. S. Bradley, M. K. Hughes, J. Overpeck, F. T. Keimig, and W. Gross, 2000: Global temperature patterns in past centuries: An interactive presentation. *Earth Interactions*, **4**(4), 1–29.
- Mann, M. E., and Coauthors, 2009: Global signatures and dynamical origins of the Little Ice Age and Medieval Climate Anomaly. *Science*, **326**(5957), 1256–1260.
- Masson-Delmotte, V., and Coauthors, 2006: Past and future polar amplification of climate change: Climate model intercomparisons and ice-core constraints. *Climate Dyn.*, **26**(5), 513–529.
- Miller, G. H., and Coauthors, 2012: Abrupt onset of the Little Ice Age triggered by volcanism and sustained by sea-ice/ocean feedbacks. *Geophys. Res. Lett.*, **39**, L02708, doi: 10.1029/2011GL050168.
- Neukom, R., and Coauthors, 2014: Inter-hemispheric temperature variability over the past millennium. *Nature Clim. Change*, **4**(5), 362–367.
- Phipps, S. J., L. D. Rotstayn, H. B. Gordon, J. L. Roberts, A. C. Hirst, and W. F. Budd, 2011: The CSIRO Mk3L climate system model version 1.0—Part 1: Description and evaluation. *Geoscientific Model Development*, **4**, 483–509.
- Ren, G. Y., 1998: Pollen evidence for increased summer rainfall in the Medieval Warm Period at Maili, northeast China. *Geophys. Res. Lett.*, **25**(11), 1931–1934.
- Schmidt, G. A., and Coauthors, 2006: Present day atmospheric simulations using GISS ModelE: Comparison to in-situ, satellite and reanalysis data. *J. Climate*, **19**, 153–192.
- Schmidt, G. A., and Coauthors, 2011: Climate forcing reconstructions for use in PMIP simulations of the last millennium (v1.0). *Geoscientific Model Development*, **4**(1), 33–45.
- Schneider, D. P., C. M. Ammann, B. L. Otto-Bliesner, and D. S. Kaufman, 2009: Climate response to large, high-latitude and low-latitude volcanic eruptions in the Community Climate System Model. *J. Geophys. Res.*, **114**, D15101, doi: 10.1029/2008JD011222.
- Swingedouw, D., L. Terray, C. Cassou, A. Voldoire, D. Salas-Mélia, and J. Servonnat, 2011: Natural forcing of climate during the last millennium: Fingerprint of solar variability. *Climate Dyn.*, **36**(7–8), 1349–1364.
- Tan, L. C., Y. J. Cai, H. Cheng, Z. S. An, and R. L. Edwards, 2009: Summer monsoon precipitation variations in central China over the past 750 years derived from a high-resolution absolute-dated stalagmite. *Palaeogeography, Palaeoclimatology, Palaeoecology*, **280**(3–4), 432–439.
- Taylor, K. E., 2001: Summarizing multiple aspects of model performance in a single diagram. *J. Geophys. Res.*, **106**(D7), 7183–7192.
- Wu, T. W., 2012: A mass-flux cumulus parameterization scheme for large-scale models: Description and test with observations. *Climate Dyn.*, **38**, 725–744.
- Yang, B., C. Qin, J. L. Wang, M. H. He, T. M. Melvin, T. J. Osborn, and K. R. Briffa, 2014: A 3,500-year tree-ring record of annual precipitation on the northeastern Tibetan Plateau. *Proceedings of the National Academy of Sciences of the United States of America*, **111**(8), 2903–2908.
- Yang, K. Q., and D. B. Jiang, 2015: Interannual climate variability of the past millennium from simulations. *Atmos. Ocean. Sci. Lett.*, **8**(3), 160–165.
- Yukimoto, S., and Coauthors, 2012: A new global climate model of the Meteorological Research Institute: MRI-CGCM3—Model description and basic performance. *J. Meteor. Soc. Japan*, **90A**, 23–64.
- Zhou, T. J., B. Li, W. M. Man, L. X. Zhang, and J. Zhang, 2011: A comparison of the Medieval Warm Period, Little Ice Age and 20th century warming simulated by the FGOALS climate system model. *Chinese Sci. Bull.*, **56**, 3028–3041.
- Zorita, E., J. F. González-Rouco, H. Von Storch, J. P. Montávez, and F. Valero, 2005: Natural and anthropogenic modes of surface temperature variations in the last thousand years. *Geophys. Res. Lett.*, **32**(8), doi: 10.1029/2004GL021563.